Appl. Phys. A (2015) 120:1375–1382
DOI 10.1007/s00339-015-9318-6

Applied Physics A
Materials Science & Processing

CrossMark

Investigation of the annealing effects on the structural and optoelectronic properties of RF-sputtered ZnO films studied by the Drude–Lorentz model

Manuel García-Méndez[1] · Álvaro Bedoya-Calle[2] · Ricardo Rangel Segura[3] · Víctor Coello[4]

Received: 28 April 2015 / Accepted: 22 June 2015 / Published online: 3 July 2015
© Springer-Verlag Berlin Heidelberg 2015

Abstract Zinc oxide films were deposited on glass substrates by RF reactive magnetron sputtering and post-annealed in vacuum at 100, 200, and 300 °C. Structural and optical properties of films were obtained using X-ray diffraction and UV–visible spectroscopy. Optical parameters were extracted from transmittance curves using the single-oscillator Drude–Lorentz model. The evolution of the optical and structural properties of films with the annealing process was investigated. The films crystallized into the hexagonal würzite lattice structure, with preferential growth along the *c*-axis [0002]. The results indicate that the crystalline quality of films improved with annealing, whereas transparency was reduced from 90 to 80 % at 300 °C. With post-annealing, the absorption edge shifted to the red, while the optical band gap decreased from $E_g = 3.28$ to $E_g = 3.26$ eV because of the Burstein–Moss effect. Calculated values of plasma frequency, w_p, fall within the IR range and decrease with temperature, from $w_p = 5.56 \times 10^{14}$ rad/s $(2950\,\text{cm}^{-1})$ to $w_p = 1.1 \times 10^{14}$ rad/s $(587\,\text{cm}^{-1})$.

✉ Manuel García-Méndez
mgarciamendez@hotmail.com; mgarcia@fcfm.uanl.mx

Álvaro Bedoya-Calle
alvaro.bedoyacl@uanl.edu.mx

[1] CICFIM de la FCFM-UANL, Manuel L. Barragán S/N Cd. Universitaria, CP 66450 S.N. de los Garza, N.L., Mexico

[2] FIME de la UANL, Av. Universidad S/N, Cd. Universitaria, CP 66450 S.N. de los Garza, N.L., Mexico

[3] División de Estudios de Posgrado, Facultad de Ingeniería Química, UMSNH, Francisco j. Mújica S/N, CP 58030 Morelia, Mich., Mexico

[4] CICESE Unidad Monterrey, Alianza Sur 203, Parque PIIT, CP 66600 Apodaca, N.L., Mexico

1 Introduction

Zinc oxide (ZnO) is a binary transparent conducting oxide (TCO) with properties of great interest due to their basic scientific research and potential technological applications [1–6]. ZnO has a würzite crystalline structure (lattice spacing $a_0 = 3.24$ Å and $c_0 = 5.20$ Å). ZnO also possesses a wide ordinary optical band gap (E_g) of ~3.3 eV, which makes it transparent in the UV–Vis–NIR region, and a large exciton binding energy (60 meV), which enhances the luminescence efficiency of light emission [1, 7, 8]. This material has garnered much commercial and scientific interest compared with other TCO films, such as indium tin oxide [9]. The numerous advantages of ZnO include the tuning of its physical properties, its low cost, its abundance in the earth, its non-toxicity, and its compatibility with large-scale processes and relative easy fabrication [5, 9–11]. Several techniques have been used to grow ZnO films, such as pulsed laser deposition [3], DC reactive magnetron sputtering [4, 5], atomic layer deposition [6], electron beam evaporation [12], sol–gel [13], and spray pyrolysis [14]. In this context, reactive radio-frequency (RF) magnetron sputtering is an attractive alternative method for growing ZnO films because of the more accurate thickness control and a higher uniformity compared with other thin-film deposition techniques [15, 16]. The properties of the ZnO films deposited by RF magnetron sputtering depend on the deposition parameters involved in the growth process, such as the RF power, sputtering gas pressure, gas flow rate, and temperature. By adjusting these processing parameters, ZnO films with properties that are compatible with optical devices may be obtained [8, 15, 16]. In regard to experimental parameters, post-annealing is a process widely used to improve the crystallinity and to reduce surface

roughness of RF-sputtered films [8, 10–12]. Applying temperature also may result in enhanced carrier concentration and higher electrical conductivity, as annealing increases the concentration of oxygen vacancies while removing chemisorbed oxygen [8].

Additionally, TCOs are emerging as possible alternative constituent materials to replace noble metals such as silver and gold for low-loss plasmonic and metamaterial (MM) applications in the near-infrared (NIR) regime. TCOs additionally offer great modulation and switching possibilities for oncoming generation of tunable plasmonic and MM devices. Recent studies have demonstrated that ZnO films are good candidates as plasmonic materials in the near-infrared frequency range, because they exhibit metallic behavior and smaller losses compared to those of silver and gold in the NIR [3, 17, 18]. By careful control and optimization of the fabrication conditions of ZnO, it is possible to grow thin films that exhibit the critical optical properties suitable for plasmonic applications in the NIR [3, 8, 18]. These applications require accurate determination of the optoelectronic parameters of the material, which include the band gap (E_g), the absorption coefficient (α), the refractive index (n), and the plasma frequency (w_p). These parameters can be conveniently determined from experimental data by applying suitable optical models [8, 18].

Given the potential applications of this type of films, precise knowledge about the effects of temperature on their structural and optical properties is an issue that still must be investigated. In this work, a set of ZnO films were prepared by RF reactive magnetron sputtering. After deposition, the films were annealed in a reducing atmosphere (argon). The ZnO films were characterized using UV–Vis spectroscopy and X-ray diffraction. From optical measurements, the envelope model and the Drude–Lorentz single-oscillator model were used to extract the optical constants of films. The effects of annealing on the structural and optical properties of films were investigated.

2 Experimental details

Zinc oxide films were deposited by reactive magnetron sputtering onto glass substrates. Cylindrical metallic zinc with a 99.9 % purity, 1″diameter and 1/8″ thickness was used as the target. Before deposition, the substrates and target were cleaned in an ultrasonic bath. The deposition chamber (bell jar) was pumped down to a base pressure of 1×10^{-6} Torr.

The gases were introduced through individual electronic mass flow meters (Aalborg). The target-substrate distance was 5 cm, and a movable shutter was placed between the target and the substrate. Plasma was then generated at an argon working pressure of 20 mTorr by applying a RF power of 50 W and 13.56 MHz. The target was sputter-cleaned for 5 min with the shutter protecting the sample. Once the sputter cleaning was completed, oxygen was introduced into the deposition chamber. The working pressure was maintained at $\sim$21 mTorr, while the oxygen and argon flow during deposition was 20 and 1 sccm, respectively. A quartz crystal oscillator monitored the thickness and deposition rate. Final coating was achieved in 15 min. After deposition, the ZnO films were subjected to thermal annealing at temperatures of 100, 200, and 300 °C under an argon atmosphere of 50 mTorr. The annealing time was fixed in each case to 1 h. The samples were allowed to cool down at room temperature (RT) while vacuum atmosphere was maintained.

For each annealing temperature, the optical and structural properties of a chosen sample were obtained. The structural properties were analyzed by XRD using a Rigaku Miniflex II diffractometer (Cu-Kα radiation). A standard θ-2θ Bragg–Brentano geometry was used for measurements, with a step size of 0.02°. Optical transmittance measurements were performed with a Thermo-Scientific Evolution 600 UV–Vis spectrophotometer. A wavelength range of 300–900 nm with a bandwidth of 1.0 nm and a data interval of 0.5 nm was used. The UV–Vis spectrophotometer is equipped with a high-precision holder device to ensure that the samples are placed in the same position prior to each analysis

3 Results and discussion

3.1 Structural characterization

Figure 1 shows the X-ray diffraction patterns before and after annealing at 100, 200, and 300 °C. In general, the XRD patterns indicate the polycrystalline nature of films. The peak assignment corresponds to a würzite structure (JCPDS file 36-1451). The most intense (002) reflection indicates a preferentially oriented film at the c-axis, perpendicular to the substrate. Annealing at higher temperatures corresponds to an improved crystallinity, as the intensity of the (002) reflection increases with the annealing temperature. Regarding this diffraction peak, the prominent (002) orientation is due to the lower surface energy of this surface compared with other planes [8, 11, 12]. This growth orientation is also achieved if the substrate is kept in a suitable position with respect to the target [11].

For RF-sputtered ZnO films deposited in similar conditions (pressure and equipment), we conducted XPS measurements in an attempt to reveal details about atomic weight ratio Zn:O. Thus, measurements revealed that with temperature (from RT to 300 °C), stoichiometry tends to approach to the ideal bulk Zn:O atomic weight proportion (not detected by XRD measurements). The non-

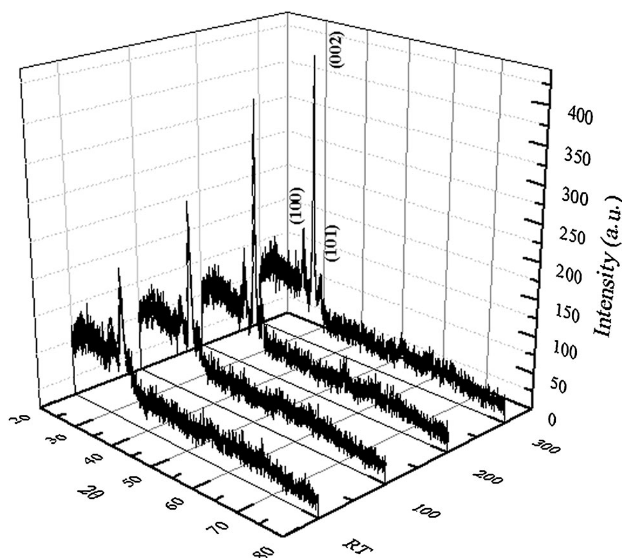

Fig. 1 X-ray diffraction patterns before and after annealing at 100, 200, and 300 °C

stoichiometry of films springs from loosely bound oxygen on the surface, other than lattice oxygen. Further details about conducted XPS analysis can be found elsewhere [19].

The Bragg equation, $2d_{hkl}\text{Sin}\theta = n$, and the distance between planes for a hexagonal lattice relation

$$d_{hkl} = \frac{1}{\sqrt{\frac{4}{3}\left(\frac{h^2+hk+k^2}{a^2}\right) + \frac{l^2}{c^2}}} \quad (1)$$

were used to obtain the lattice parameters from the diffractograms. Afterward, a multiple correlation analysis was performed by using a least-squares minimization. The initial values of a_0 and c_0 were taken from the JCPDS standards and introduced as fitting variables. Furthermore, the crystallite size, L, was estimated through the Scherrer formula, using the FWHM of the (002) peak.

The structural parameters obtained as a function of temperature are summarized in Table 1. The annealing produced an enhancement of both the XRD peak intensity and the crystallite size. The intensity of the (002) diffraction peak is the highest at 300 °C along with the smallest line width, which indicated that the best crystallinity of ZnO was observed at this temperature.

Table 1 Summary of the structural parameters before and after annealing at 100, 200, and 300 °C. (JCPDS file # 36-1451, $a_0 = 3.24$ Å, $c_0 = 5.20$ Å; $2\theta = 34.42°$)

T (°C)	a_0 (Å)	c_0(Å)	2θ (°)	Γ (°)	L (nm)
RT	3.28	5.28	33.91	1.36	6.3
100	3.27	5.26	34.10	1.18	7.2
200	3.25	5.20	34.44	0.73	11.7
300	3.24	5.20	34.42	0.70	12.2

Regarding the X-ray diffractograms, the angle 2θ of the (002) reflection is lower than that of the bulk value 34.4°, and the lattice constants a_0 and c_0 are elongated compared to the stress-free ZnO powder (the powder standard has an "ideal" lattice parameter because powders, unlike thin films, are not subjected to an internal and/or substrate-film stress). Thus, the strain is positive and the stress is compressive [12, 13]. With annealing, the diffraction angle 2θ shifts toward higher values, while the lattice parameters decrease in value. Between 200 and 300 °C, the lattice parameters approached the values of the ZnO standard.

Therefore, annealing helped to release compressive stress, which results in an improved preferential c-growth while allowing for the small crystallites to coalesce and form larger crystallites in the würzite phase [8, 10, 11].

3.2 Optical characterization

Figure 2 shows the transmittance spectra in the wavelength range of 300–850 nm, before and after annealing at 100, 200, and 300 °C. The optical band gap (E_g) was obtained by the Tauc method (inset).

At the onset of the absorption edge, the absorption coefficient α can be calculated from the relation:

$$\alpha = \frac{1}{d}Ln\left[\frac{100}{T(h\nu)}\right] \quad (2)$$

where T is the measured transmittance and d is the optical thickness. The optical thickness and refractive index, n, are extracted from T using the envelope method [20, 21]. Then,

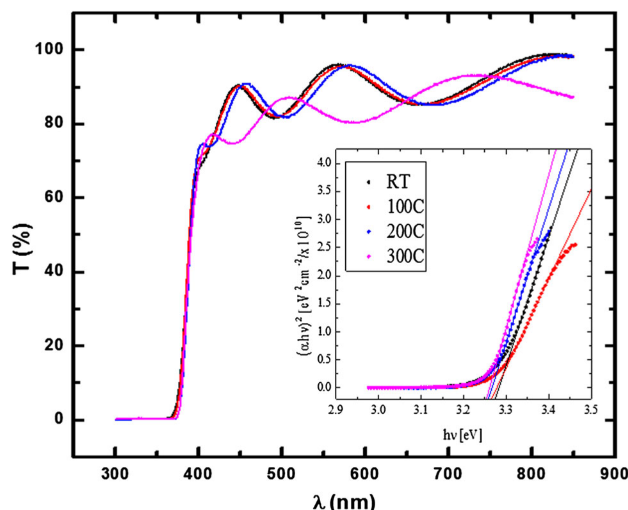

Fig. 2 Transmittance spectra before and after annealing at 100, 200, and 300 °C. *Inset* Tauc curves

the refractive index of films was modeled by a Cauchy dispersion Eq. [8, 9, 22]:

$$n(\lambda) = A_0 + \frac{A_1}{\lambda^2} + \ldots \quad (3)$$

where $A_0, A_1, \ldots$ are constants.

The optical band gap, E_g, was extracted from Tauc's relation:

$$(\alpha h\nu)^2 = A(h\nu - E_g) \quad (4)$$

where A is the edge width parameter. The value of E_g is obtained by plotting $(\alpha h\nu)^r$ versus $h\nu$ with $r = 2$ for a direct transition [2, 4, 12]. The optical parameters obtained as a function of temperature are summarized in Table 2.

From the data presented, the average transmittance over the visible wavelength ($\sim$400–750 nm) was observed to be very similar for all samples, with a value higher than 80 %. A slight decrease in transmittance was detected at 300 °C. In addition, all samples exhibited sharp absorption edges at 380–400 nm.

Alternatively, the interference fringes, characteristic of dielectric films, can be used as a qualitative criterion to evaluate the film quality. In Fig. 2, the fringes detected at RT and at 100, 200, and 300 °C indicate a homogeneous thickness. At 300 °C, the decrease in the transmittance and the shrinkage of the interference fringes can be attributed to an increased surface roughness, which can cause an increase in the optical scattering [12].

At the extremes of the annealing regime (RT and 300 °C), it can be observed that the optical thickness of sample decreases with increase in annealing temperature, as expected for thin films. However, in the middle (100 and 200 °C), thickness vary. At 100 and 200 °C, the process is governed by temporary mechanisms of diffusion and crystalline rearrangement. Thus, the annealing can induce formation of non-stoichiometric metallic-oxide domains, in addition to roughness at surface, both factors adding up dispersion effects before sample recrystallizes at 300 °C. Hence, the dispersion effects induce changes in the interference fringes (mainly close to the middle wavelength region) from which the optical thickness is extracted.

The absorption edge values were observed to depend on the temperature. The obtained band gap at $\sim$3.28–3.26 eV is comparable to the values reported for ZnO thin films deposited by RF [8, 11, 15, 23].

As a function of temperature, the band gap shifts to lower values. This red shift, known as the Burstein–Moss shift (where the shift also occurs at the blue), is a result of the dependence of the optical band gap on the carrier concentration. ZnO is an intrinsic material whose optical properties close to the fundamental band edge are strongly affected by excitonic interaction [5]. In the film at RT, the process of phase formation has not been completed and metallic unreacted species or oxygen vacancies can produce unintentionally introduced donor centers, which produce shallow donor or impurity states located close to the conduction band. When temperature is increased, improvement in crystal quality tends to remove such donor centers. As a result, the carrier concentration N_c decreases and the band gap shifts to lower values. It has been reported that for ZnO films, depending on the annealing regime (temperature and atmosphere), a narrowing of the band gap (red shift) or widening of the band gap (blue shift) can be expected [11]. This reduction in N_c with annealing can be attributed to the fact that at RT, the process of phase formation has not been completed and the metallic unreacted species or oxygen vacancies can produce unintentionally introduced donor centers, which produce shallow donor or impurity states located close to the conduction band.

The highest contribution to N_c at RT may be due to excess zinc, acting as a shallow donor. Such unintentionally induced donors on oxygen-deficient non-stoichiometric ZnO films produced by RF sputtering deposition have been reported [24]. When the annealing temperature is increased, improvement in the crystal quality removes structural defects, with a reduction in N_c.

Figure 3 shows the absorption coefficient as a function of energy. The values of $\alpha(E)$ at the absorption zone, between $18{,}000\ \mathrm{cm}^{-1} < \alpha < 150{,}000\ \mathrm{cm}^{-1}$, were found to be similar to those of ZnO films deposited by sol–gel [2] and RF plasma [8, 23].

Dispersion curves before and after annealing at 100, 200, and 300 °C are shown in Fig. 4. For all of the curves, the refractive index was found to increase with lower wavelengths. In addition, the refractive index remains almost constant in the visible and NIR wavelength ranges.

Table 2 Summary of optical parameters before and after annealing at 100, 200, and 300 °C

T (°C)	t (nm)	E_g (eV)	ε_L	ε_{opt}	$\frac{N}{m^*}$ (10^{56}/m^{3}kg)	E_d (eV)	E_0	w_p (10^{14} rad/s)	ν (10^{13} Hz)	ν (cm^{-1})	N (10^{19}/cm^3)
RT	475	3.28	4.16	3.80	4.05	22.4	8	5.56	8.85	2950	10
100	416	3.27	4.07	3.84	2.49	22.6	7.94	4.33	6.9	2300	6.3
200	487	3.26	4.06	3.86	2.14	22.6	7.92	4.01	6.38	2127	5.4
300	432	3.26	5.23	5.21	0.22	27.5	6.52	1.1	1.76	587	0.5

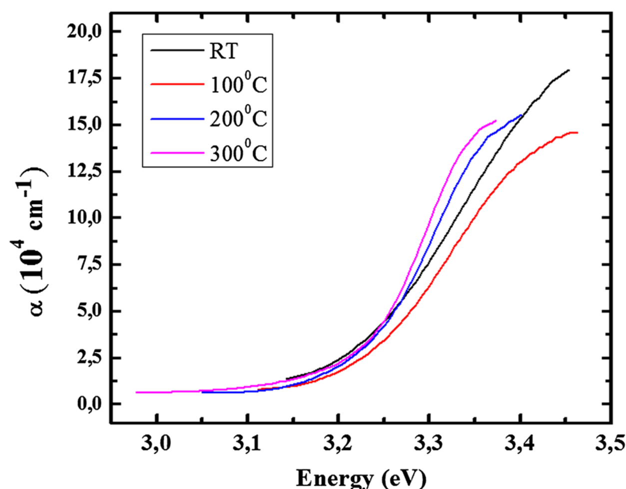

Fig. 3 Absorption coefficient as a function of energy before and after annealing at 100, 200, and 300 °C

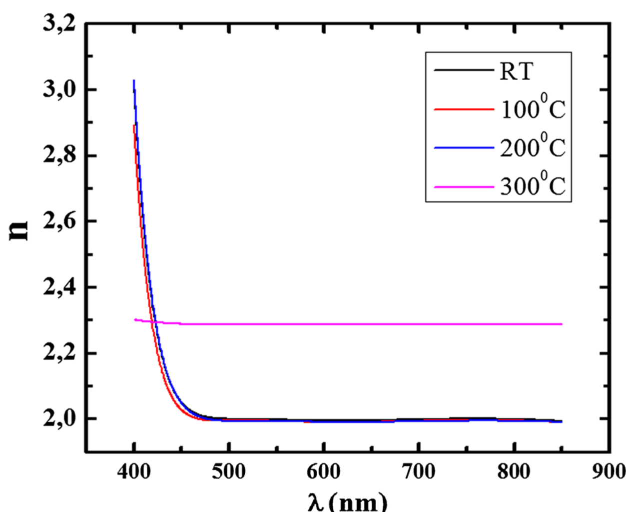

Fig. 4 *Dispersion curves* before and after annealing at 100, 200, and 300 °C

This trend fits to the Kramers–Kröning relationships for normal dispersion [22, 25]. At $\lambda = 550$ nm, $n \approx 2.0$ for RT, 100 and 200 °C, while $n \approx 2.1$ at 300 °C. Thus, the variation in dispersion reflects a critical dependence on temperature because at RT, 100 and 200 °C, the dispersion curves exhibit little variation. The decrease in transmittance and the increase in scattering associated with structural disorder, chemical defects, surface roughness and the effect of grain boundaries can explain the differences in dispersion observed at 300 °C, as a higher refractive index indicates a higher dispersion. In addition, higher dispersion can contribute to a reduced transmittance.

Additionally, the fundamental electronic excitation spectrum of a substance can be analyzed in terms of the frequency-dependent dielectric constant $\varepsilon_r(w)$:

$$\varepsilon_r(w) = \varepsilon_1(w) + i\varepsilon_2(w) \tag{5}$$

By applying the Drude oscillator modified to semiconductors, the frequency dependence of the dielectric constant $\varepsilon_r(w)$ is given by [6, 22]:

$$\varepsilon_r(w) = \varepsilon_{\text{opt}} - \frac{Ne^2}{m^* \varepsilon_0} \frac{1}{(w^2 + i\gamma_p w)} \tag{6}$$

where $\varepsilon_\infty \equiv \varepsilon_{\text{opt}}$ is the high-frequency dielectric constant measured in the transparent spectral region, below the interband absorption edge, $\gamma_{\text{p}} = \frac{1}{\tau_{\text{p}}}$ (τ_{p} damping time), m^* is the effective mass that accounts for the band structure of the semiconductor, and

$$w_p^2 = \frac{Ne^2}{\varepsilon_{\text{opt}} \varepsilon_0 m^*} \tag{7}$$

is the plasma frequency. For semiconductors, w_{p} occurs at frequencies in the IR spectral range [3, 18, 22].

The refractive index dispersion of samples was evaluated according to the single-oscillator model developed by Wemple and Domenico [25]. This model depicts the dielectric response for transitions below the optical band gap. In this model, the values of E_d and E_0 are related to the refractive index as:

$$\frac{1}{n^2 - 1} = \frac{E_0}{E_d} - \frac{1}{E_0 E_d} (hv)^2 \tag{8}$$

where E_0 is the average excitation energy for electronic transitions and E_d is the dispersion energy, which is a measure of the average strength of the oscillator. In Eq. (8), E_d is related to $\varepsilon_1(w)$ at high frequencies above the $\varepsilon_2(w)$ cutoff.

By plotting $\frac{1}{n^2-1}$ versus $\frac{1}{(hv)^2}$ and fitting a straight line, the value of E_0, E_d can be obtained. By considering the real part of the dispersion, $n^2 = \varepsilon_\infty = \varepsilon_r(\infty)$.

Conversely, in the low-frequency limit, $\varepsilon_r(0) = \varepsilon_L$, where ε_L is the static dielectric constant related to the lattice contribution.

Using the formula

$$\varepsilon_\infty = \varepsilon_L - \frac{e^2}{\pi c^2} \frac{N}{m^*} \lambda^2. \tag{9}$$

by plotting n^2 versus λ^2 and fitting a straight line, the values of ε_L and $\frac{N}{m^*}$ can be obtained, where $\frac{N}{m^*}$ is the ratio of the carrier concentration to the electron effective mass.

Once the lattice parameters, $\frac{N}{m^*}$, and E_{g} are known, the bulk effective mass, m^*, was obtained through [7, 26]:

$$\frac{m}{m^*} = 1 + \frac{p^2}{2mE_{\text{g}}} \tag{10}$$

where m is the free electron mass, $\mathbf{p} = \hbar \mathbf{K}$, and $|\mathbf{K}| = \pi\sqrt{\frac{2}{a_0^2} + \frac{1}{c_0^2}}$ is the magnitude of the shortest reciprocal lattice

vector with lattice constants a_0 and c_0 [27]. In this formula, a parabolic behavior in the band structure at $\Gamma = 0$ and a constant momentum p (momentum matrix element) are assumed.

According to the theoretical results, the band structure of hexagonal ZnO shows high-symmetry lines in the hexagonal Brillouin. Both the valence band maxima and the lowest conduction band minima occur at the Γ point. Therefore, ZnO is a semiconductor with a direct band gap [10].

Figure 5 shows an exemplary plot of n^2 versus λ^2 for the as-deposited sample, from which the static dielectric constant, ε_L, was obtained. At long wavelengths, a region of linearity is extended enough to allow determination of ε_L and $\frac{N}{m^*}$. At short wavelengths, a positive curvature deviation due to the proximity of the band edge or excitonic absorption can be observed.

Figure 6 shows the plot of $\frac{1}{n^2-1}$ versus $\frac{1}{\lambda^2}$ for the as-deposited sample, from which the optical constant, $\varepsilon_{\mathrm{opt}}$, was obtained. At long wavelengths, a region of linearity is extended enough to allow for determination of $\varepsilon_{\mathrm{opt}}$, E_0 and E_d. At short wavelengths, a negative curvature deviation due to the proximity of the band edge or excitonic absorption can be observed.

As a function of temperature, the values of ε_L and $\varepsilon_{\mathrm{opt}}$ exhibit little variation from RT to 200 °C. At 300 °C, both values exhibit a remarkable change. However, at all temperatures, $\varepsilon_L > \varepsilon_{\mathrm{opt}}$. This observation implies that the refractive index gradually increases as it goes to the resonance region or the proximity of the band edge, in agreement with the Kramers–Kröning relationships for normal dispersion [22, 25]. Values of $\varepsilon_{\mathrm{opt}}$ of 3.4 [3] and 3.58–4.9 [7] for ZnO thin films have been reported in other works,

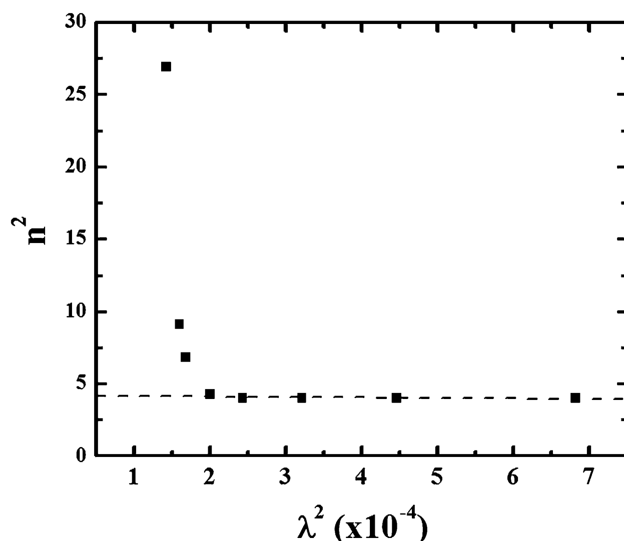

Fig. 5 Plot of n^2 versus λ^2 for the film at RT

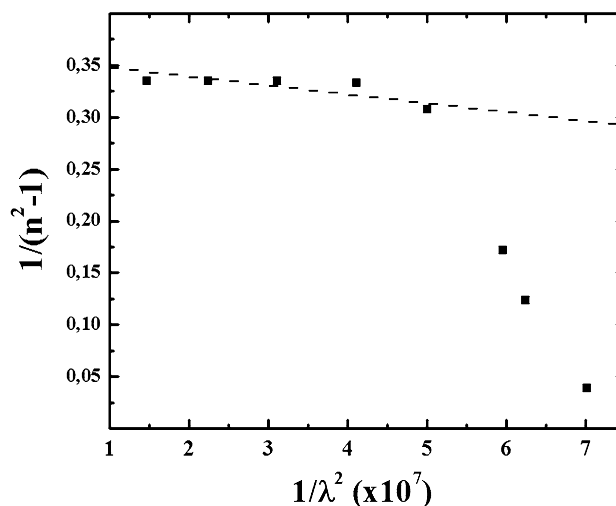

Fig. 6 Plot of $\frac{1}{n^2-1}$ versus $\frac{1}{\lambda^2}$ for the film at RT

which are consistent with our results. However, as $(\varepsilon_L - \varepsilon_{\mathrm{opt}}) \propto \frac{N}{m^*}$, a gradual decrease in the $\frac{N}{m^*}$ratio with annealing is expected (see Table 2).

Values of E_d (interband strength parameter) and E_0 (dipole oscillator parameter) exhibit the highest variation between 20 and 300 °C, with E_d being the most noted. In this case, it has been empirically found that E_d exhibits a dependence on coordination number of atoms and valence and little dependence on the band gap [14, 25]. Thus, the change in E_d can be attributed to an increase in the lattice disorder that ultimately induces changes in the electronic distribution. Although a straight comparison is not possible, it is useful to consider the earlier report of Wemple and Domenico [25], where they found for bulk ZnO values of 17.1 and 6.4 eV for E_d and E_0, respectively; note that for würzite and several oxides, (i) $E_d > E_0$ and (ii) $E_g \approx 2E_0$. Findings (i) and (ii) are confirmed in our work.

Regarding the $\frac{N}{m^*}$ ratio, the authors [14], using the envelope and Wemple–DiDomenico models, found for ZnO films (pure and metal-doped, grown by spray pyrolysis) a $\frac{N}{m^*}$ ratio on the order of $10^{56}/\mathrm{m}^3$ kg, that closely agrees with our results.

The calculated values of w_{p} (plasma frequency), $\frac{m^*}{m}$, and N (electronic concentration) are listed in Table 2. The plasma frequency for as-deposited and annealed films falls within the mid-IR range ($\sim$6000 to 300 cm^{-1}). This range agrees with the values of plasma frequency expected for metal-oxide semiconductors [23] and for ZnO films reported in other works [7, 14]. At RT and all annealing temperatures considered in this study, a bulk effective mass of $\sim$0.28 m was calculated, in close resemblance with the reported values for ZnO [28–30].

With the effective mass calculated through Eq. (10), an electronic concentration of $\sim 10^{19}/\mathrm{cm}^3$ was obtained.

With annealing, improvement in the crystal quality removes unintentionally added donor centers, resulting in a decrease in the carrier concentration. A decrease in the electronic concentration implies a reduced interaction of electrons with lattice vibrations. Therefore, the plasma frequency decreases with temperature. At 300 °C, the sample showed the best crystal quality but also the highest dispersion.

4 Conclusions

Zinc oxide thin films were deposited on glass substrates using RF reactive magnetron sputtering. The effect of annealing on the structural and optical properties for an RF-sputtered ZnO film was investigated. Optical models allowed estimating the optoelectronic properties of film and their evolution with temperature. Annealing in argon atmosphere at 100 and 200 °C improved the microstructural properties, allowing preferential growth along the (002) direction. As the annealing temperature increased, the absorption edge shifted to the red, narrowing the band gap from 3.28 to 3.26 eV. Annealing induces a thermal activation that removes the unintentionally introduced donor centers, giving as a result a decrease in the values of plasma frequency and carrier concentration.

Acknowledgments CONACyT México (Grant 168234) and PAICyT-UANL (Grant CE671-11) financed this work.

References

1. H. Dondapati, K. Santiago, A.K. Pradhan, Influence of growth temperature on electrical, optical and plasmonic properties of aluminium: zinc oxide films grown by radio frequency. J. Appl. Phys. **114**, 143506-1–6 (2013)
2. Y. Ammaih, A. Lfakir, B. Hartiti, A. Ridah, P. Thevenin, M. Siadat, Structural, optical and electrical properties of ZnO: Al thin films for optoelectronic applications. Opt. Quantum Electron. **46**, 229–234 (2014)
3. E. Sachet, M.D. Losego, J. Guske, S. Franzen, J.P. Maria, Mid-infrared surface plasmon resonance in zinc oxide semiconductor. Appl. Phys. Lett. **102**, 051111-1–4 (2013)
4. M. Suchea, S. Christoulakis, K. Moschovis, N. Katsarakis, G. Kiriakidis, ZnO transparent thin films for gas sensor applications. Thin Solid Films **515**, 551–554 (2006)
5. S. Logothetidis, A. Laskarakis, S. Kassavetis, S. Lousinian, C. Gravalidis, G. Kiriakidis, Optical and structural properties of ZnO for transparent electronics. Thin Solid Films **516**, 1345–1349 (2008)
6. A. Frölich, M. Wegener, Spectroscopic characterization of highly doped ZnO films grown by atomic layer deposition for three dimensional infrared materials. Opt. Mater. Express **1–5**, 883–889 (2011)
7. R.N. Gayen, K. Sarkar, S. Hussain, R. Bhar, A.K. Pal, ZnO films prepared by modified sol–gel technique. Indian J. Pure Appl. Phys **49**, 470–477 (2011)
8. M.F. Al-Kuhaili, S.M.A. Durrani, I.A. Bakhtiari, M. Saleem, Optical constants of vacuum annealed radio frequency (RF) magnetron sputtering. Opt. Commun. **285**, 4405–4412 (2012)
9. Y. Yang, X.W. Sun, B.J. Chen, C.X. Xu, T.P. Chen, C.Q. Sun, B.K. Tay, Z. Sun, Refractive indices of textured indium tin oxide and zinc oxide thin films. Thin Solid Films **510**, 95–101 (2006)
10. S. Youssef, P. Combette, J. Podlecki, R. Al Asmar, A. Foucaran, Structural and optical characterization of ZnO thin films deposited by reactive RF magnetron sputtering. Cryst. Growth Design **9–2**, 1088–1094 (2009)
11. M. Bouderbala, S. Hamzaoui, M. Adnane, T. Sahraoui, M. Zerdali, Annealing effect on properties of transparent and conducting ZnO thin films. Thin Solid Films **517**, 1572–1576 (2009)
12. A. Mahmood, N. Ahmed, Q. Raza, T.M. Khan, M. Mehmood, M.M. Hassan, N. Mahmood, Effect of thermal annealing on the structural and optical properties of ZnO thin films deposited by the reactive e-beam evaporation technique. Phys. Scr. **82**, 065801 (2010). (8p)
13. M.R. Khanlary, S. Isazadeh, Structural and optical properties of ZnO thin films prepared by sol–gel method. Micro Nano Lett. **6–9**, 767–769 (2011)
14. D.K. Madhup, D.P. Subedi, A. Huczko, Influence of doping on optical properties of ZnO nanofilms. Optoelectron. Adv. Mater. **4–10**, 1582–1586 (2010)
15. S.-S. Lin, J.-L. Huang, D.-F. Lii, The effects of r.f. power and substrate temperature on the properties of ZnO films. Surf. Coat. Technol. **176**, 173–181 (2004)
16. J. Kim, M.-C. Kim, J. Yu, K. Park, H2/Ar and vacuum annealing effect of ZnO thin Films deposited by RF magnetron sputtering system. Curr. Appl. Phys. **10**, S495–S498 (2010)
17. J. Kim, Y. Zhao, G.V. Naik, N.K. Emani, U. Guler, A.V. Kildishev, A. Alu, A. Boltasseva, Nanostructured transparent conductive oxide films for plasmonic applications. CLEO:2013 Technical Digest, OSA (2013)
18. D.C. Look, K.D. Leedy, ZnO plasmonics for telecommunications. Appl. Phys. Lett. **102**, 182107 (2013)
19. M. García-Méndez, R. Rangel Segura, V. Coello, E. Martínez-Guerra, Á. Bedoya-Calle, The influence of Ce doping on the structural and optoelectronic properties of RF-sputtered ZnO films. Opt. Quantum Electron. (2015). doi:10.1007/s11082-015-0145-y
20. J.C. Manifacier, J. Gasiot, J. Fillard, A simple method for the determination of the optical constants n, k and the thickness of a weakly absorbing thin film. J. Phys. E Sci. Inst. **9**, 1002–1004 (1976)
21. R. Swanepoel, Determination of the thickness and optical constants of amorphous silicon. J. Phys. E Sci. Inst. **16**, 1214–1222 (1983)
22. M. Fox. Optical properties of Solids. Oxford University Press. 2nd ed. New York. ISBN 978-0-19-957337-0 (2011)
23. B.L. Zhu, J. Wang, S.J. Zhu, J. Wu, R. Wu, D.W. Zeng, C.S. Xie, Influence of hydrogen introduction on structure and properties of ZnO thin films during sputtering and post annealing. Thin Solid Films **519**, 3809–3815 (2011)
24. H. Nanto, T. Minami, S. Shooji, S. Takata, Electrical and optical properties of zinc oxide thin films prepared by rf magnetron sputtering for transparent electrode applications. J. Appl. Phys. **55–4**, 1029–1034 (1984)
25. S.H. Wemple, M. DiDomenico Jr, Behavior of the electronic dielectric constant in covalent and ionic materials. Phys. Rev. B **3–4**, 1338–1351 (1971)
26. D. Bhattacharyya, S. Chaudhuri, A.K. Pal, Determination of effective mass of electrons in ternary compound semiconductors. Vacuum **46–1**, 1–3 (1995)
27. D. Cheng, M. Zhang, J. Chen, Ch. Yang, X. Zeng, D. Cao, Computer screening of dopants for the development of new SnO2

based transparent conducting oxides. J. Phys. Chem. C **118**, 2037–2043 (2014)

28. M. Oshikiri, Y. Imanaka, F. Aryasetiawan, G. Kido, Comparison of the electron effective mass of the n-type ZnO in the wurtzite structure measured by cyclotron resonance and calculated from rst principle theory. Phys. B **298**, 472–476 (2001)
29. Y. Imanaka, M. Oshikiri, K. Takehana, T. Takamasu, G. Kido, Cyclotron resonance in n-type ZnO. Phys. B **298**, 211–21 (2001)
30. Z.H. Zhanga, M. Heb, Q. Li, Obtaining the effective electron mass from valence electron energy-loss spectroscopy. Solid State Commun. **149**, 1856–1859 (2009)